Fuel 428 (2027) 140168

Contents lists available at ScienceDirect

Fuel

journal homepage: www.elsevier.com/locate/fuel

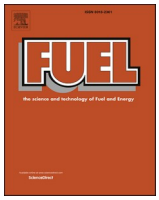

Full Length Article

Electrochemical hydrogenation of the hydrophobic oily phase of pinewood and wheat-straw pyrolysis oils in methanol☆

Cesar Catizane [a,*], Ying Jiang [b], Scott Banks [c], Joy Sumner [d], Stefano Mori [a]

[a] Energy and Sustainability Theme, Cranfield University, Cranfield MK43 0AL, UK
[b] Renewable and Sustainable Energy Research Centre, Technology Innovation Institute, Abu Dhabi, United Arab Emirates
[c] College of Engineering and Physical Sciences, Aston University, Birmingham B4 7ET, UK
[d] Franco-Australian Centre for Energy, Swinburne University of Technology, Melbourne, Australia

A B S T R A C T

Efficient electrochemical hydrogenation (ECH) of organic compounds is essential for sustainability, promoting chemical feedstock circularity and synthetic fuel production. Yet in bio-oil, phase separation in aqueous media restricts ECH to the aqueous fraction and leaves the hydrophobic oily phase comparatively inaccessible. Herein, we test whether methanol catholytes can directly engage the hydrophobic oily phase of pinewood and wheat-straw pyrolysis oils in an H-type cell. Using a PtRu/ACC cathode with NaCl or TBAHFP dosed by mass, we tracked composition as internal-standard-normalised GC–MS responses with qualitative FTIR support and assessed cathode condition by SEM/EDS. Phenolic responses decreased preferentially; FTIR indicated reduced aromatic character with condition-dependent O–H and aliphatic C–H envelopes, and additive choice set a trade-off with surface condition. This paper establishes chemical tractability of oily-phase ECH in methanol under mild conditions and identifies additive-dependent degradation as a dominant practical constraint.

1. Introduction

Upgrading pyrolysis bio-oil matters because its high oxygen content, acidity, and instability limit direct use [1,2], whereas electrochemical hydrogenation (ECH) offers a mild, electrified route to stabilise and deoxygenate organics [3,4]. Yet in bio-oil, aqueous electrolytes favour the aqueous fraction: phase separation leaves the hydrophobic oily phase comparatively inaccessible despite its phenolic and aromatic richness. Efficient ECH of organic compounds is therefore both a sustainability opportunity and a phase-compatibility problem.

Beyond ECH, conventional upgrading includes hydrotreating/hydrodeoxygenation with pressurised H_2 at elevated temperature and pressure, catalytic cracking or catalytic pyrolysis over acidic zeolites, and stabilisation via derivatisation [5–9]. ECH is attractive because it operates at low temperature and ambient pressure and can be powered by renewable electricity.

Early ECH work established fundamentals using model compounds, ranging from phenolics to simple acids and alcohols, across a variety of electrode materials and solvents, mapping intrinsic reactivity and selectivity under controlled, single-phase conditions [5,10–14]. Building on that, researchers then tackled whole condensates in the aqueous phase at low temperature and ambient pressure, achieving partial stabilisation of water-soluble fractions but leaving the hydrophobic oil largely unaddressed [15–17]. Only more recently has the field attempted direct treatment of the oily phase itself, and those demonstrations have relied on elevated temperature and pressure to overcome phase transfer and mass transport limits [18]. In this paper, we close that gap by directly engaging the hydrophobic oily phase under mild conditions, without resorting to high temperature or pressure, showing that it can be selectively engaged in situ. This matters because it preserves the low energy, low complexity advantages that make ECH attractive, while targeting the fraction rich in aromatics and associated with instability, thereby moving ECH closer to direct engagement of the oily phase under mild conditions, while identifying electrode durability as a key constraint to be resolved for practical deployment.

We frame the study around two coupled aims: to maximise upgrading of the oily phase under mild conditions and to minimise electrode degradation. Degradation matters because it drives operating costs and limits scalability through shorter electrode lifetimes and downtime for maintenance. In media relevant to oily phase work, chloride and other ions can adsorb or participate in side reactions at metal surfaces, and solvent-salt combinations can alter the reaction environment in ways that jeopardise durability. [19].

This study targets that gap with three aims: to test whether a

☆ This article is part of a special issue entitled: '3rd FERIA' published in Fuel.

* Corresponding author.
E-mail address: cesar.catizane@cranfield.ac.uk (C. Catizane).

https://doi.org/10.1016/j.fuel.2026.140168
Received 4 November 2025; Received in revised form 17 April 2026; Accepted 30 May 2026
Available online 13 June 2026
0016-2361/© 2026 The Author(s). Published by Elsevier Ltd. This is an open access article under the CC BY license (http://creativecommons.org/licenses/by/4.0/).

methanol catholyte can solvate and bring the oily phase of wheat-straw and pinewood bio-oils into electrochemical contact in an H-type cell; to compare an inorganic (NaCl) and a bulky organic (tetrabutylammonium hexafluorophosphate, TBAHFP) supporting salt under otherwise similar conditions; and to relate compositional change to cathode condition so that reactivity can be weighed against surface stability. Methanol is chosen to solvate the oily fraction while remaining electrochemically compatible with typical bio-oil constituents. [18].

Here we evaluate composition by internal-standard-normalised GC–MS with FTIR support and assess cathode condition by SEM/EDS. The results identify additive-dependent trade-offs and establish that oily-phase ECH in methanol is feasible under mild conditions, while flagging conductivity-additive corrosion as a practical constraint.

2. Experimental

2.1. Materials

Sulfuric acid solution (5 M), methanol (for HPLC), and guaiacol (99%) were purchased from Thermo Fisher Scientific. Sodium chloride (ACS reagent, ≥99.0%) and tetrabutylammonium hexafluorophosphate (purum, ≥98.0% (CHN)) were purchased from Sigma Aldrich. All chemicals were used as received without further purification.

A Nafion 117 membrane (from Ion Power Inc. PA, USA) was used as the cation exchange membrane to separate the cathode and anode chambers. To ensure the activation of the membrane and optimise its ion transport capability, it was pretreated according to Peng *et al* [20]. It was treated in hydrogen peroxide (H_2O_2) at 80 °C, followed by deionized water and 1.0 M H_2SO_4 at the same temperature. Each step duration was 1 h, and the membrane was washed with deionised water after each step.

2.2. Electrochemical hydrogenation

A two-chamber electrochemical cell, separated by a cation exchange membrane (CEM) was selected for the ECH process (See Fig. 1). The selected catalytic cathode was 4 mg/cm^2 platinum ruthenium black-carbon cloth electrode and the counter electrode was a platinum plate (1x1 cm, Ossila). For all experiments, the anode chamber was filled with 90 mL of 1.0 M sulfuric acid and the catholyte was 90 mL of methanol, and 1.5 g of either NaCl or TBAHFP was added to the cathode chamber, to increase the conductivity of methanol. Under the mass-based dosing used here, NaCl ≈ 0.29 M whereas TBAHFP ≈ 0.04 M in methanol (1.5 g per 90 mL). Therefore, observed differences reflect both ion identity and ionic strength. Matching molar concentrations would introduce practical constraints: 0.29 M TBAHFP would require ≈10 g per 90 mL, approaching the solubility limit and increasing the cost of the process, while 0.04 M NaCl would reduce conductivity approximately sevenfold in methanol, a solvent whose ionic conductivity is already limited by its low dielectric constant (ε ≈ 32.7), potentially compromising galvanostatic control [21]. The mass-based dosing used here therefore reflects a practical choice to compare both additives under workable conditions, and the present results provide a first indication of how additive class influences both conversion and electrode condition.

The tests were run under galvanostatic control (25.0 mA/cm^2) at 55 °C, conditions optimised for ECH of phenolic substrates in our previous work [22]. These parameters were held constant here to isolate the effects of the methanol solvent and supporting-electrolyte identity on oily-phase conversion and cathode stability, which are the primary variables under investigation. The cell was pre-polarised for 10 min without the bio-oil. The potentiostat maintained the set current throughout all runs without reaching its compliance voltage limit. After that, 1 mL of the oily phase was added to the system. Geometric cathode area = 4.0 cm^2; Total charge per run was calculated according to Eq.(1), where J is the current density, A is the geometric cathode area and t is time.

$$\mathbf{Q = j^*A^*t} \tag{1}$$

Considering a Faradaic efficiency (FE) of 100%, and an average compound concentration of 0.125 mol/L, to achieve 100% conversion, the duration (t) would be equal to 18.01 h (2). Where F is the Faraday constant (96 485C/mol), i is the current and n is the number of electrons needed for the hydrogenation of one molecule (n = 6 for the conversion of phenol into cyclohexanol, for example).

$$\mathbf{FE}(\%) = \frac{\mathbf{molproduced^*n^*F}}{\mathbf{i^*t}} \tag{2}$$

The experiment was run in triplicates for 20 h to ensure the availability of enough charge in the system for the conversion of the compounds. Immediately after electrolysis, 1.00 mL of catholyte was withdrawn and diluted in 2.00 mL of dichloromethane. Guaiacol internal standard (IS) was added post-sampling (0.10 mL of a 1.12 g/mL stock) to the mixture, yielding a final IS level of 0.036 g/mL (≈0.29 M) in 3.10 mL total volume; the same IS level was used for all injections. The IS level was chosen to keep all target responses within the detector's

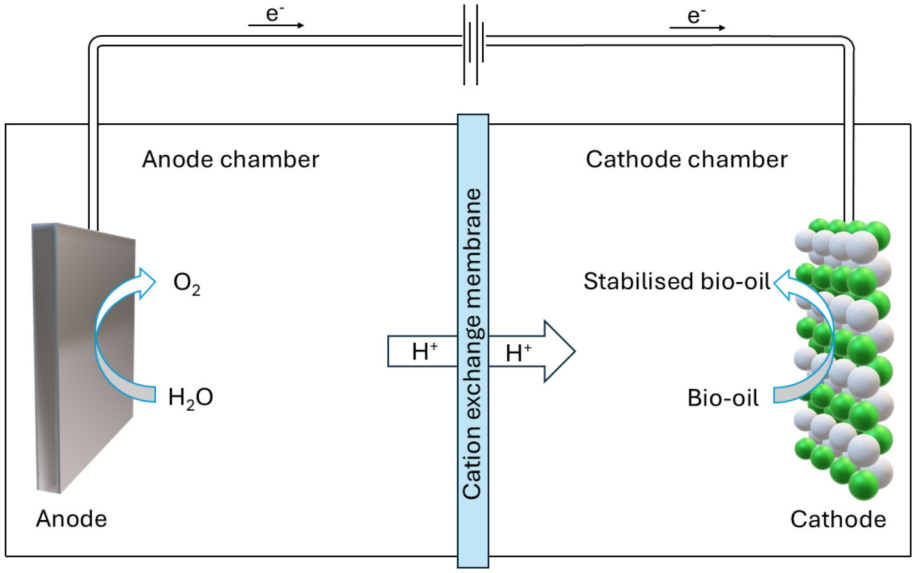

Fig. 1. Schematic representation of an H-type cell for ECH. The cell is composed of two chambers separated by a cation exchange membrane.

linear range under split 1:25; no IS saturation or detector overload was observed.

After each experiment, the electrolyte was discarded, the cell cleaned and the cathode was soaked in 5 mL dichloromethane (DCM) for 15 min, to ensure the desorption of any molecules on its surface.

2.3. Supporting electrolytes

Neat methanol was used as the catholyte to solvate the hydrophobic oily fraction while maintaining electrochemical compatibility with typical bio-oil constituents. The operating temperature was held at 55 °C, well below methanol's boiling point (64.7 °C at atmospheric pressure), to minimise solvent loss. The cell was sealed and any methanol vapour condensed on the interior walls, returning to the catholyte; no appreciable volume change was observed over the 20 h runs.

Sodium chloride (NaCl), a commonly used supporting electrolyte, provides high conductivity in methanol but introduces chloride, which under some conditions can adsorb at metal surfaces and may accelerate corrosion; PtRu/ACC is not entirely immune to chloride-assisted pitting and crevice attack [19,23]. Conversely, quaternary ammonium salts such as tetrabutylammonium hexafluorophosphate (TBAHFP) are often regarded as relatively benign towards noble metals in alcohol media, including Pt and Ru; the PF_6^- anion is typically weakly coordinating and not considered inherently corrosive [19,24]. We therefore evaluated both additives at comparable practical loadings (dosed by mass), holding all other conditions constant, and assessed composition and electrode surface condition alongside cell performance.

2.4. Biomass pyrolysis

Slow pyrolysis experiments were conducted in a screw auger reactor with a capacity of 100–200 kg/h, depending on feedstock density. The system included a feeding unit, pyrolysis reactor, vapour condensation and collection system, and char cooling and outlet. Pinewood and wheat straw were processed at average temperatures of 500 ± 5 °C and 550 ± 5 °C, respectively, with a 20-minute residence time. Vapours and gases exited the reactor via heated pipes to a spray quench column using ISOPAR™ as the quenching medium. Condensed products were collected and separated into organic and aqueous phases, while aerosols were coalesced in an electrostatic precipitator.

2.5. Analysis

The samples were taken for analysis in the GC–MS Shimadzu TQ8040. The GC used a Restek Rtx-5 capillary column, 28.5 m × 0.25 mm with a 0.25 μm film thickness, a 1.18 mL/min helium carrier gas flow rate, and a split ratio of 1: 25. The injector temperature was set at 250 °C. The GC oven program started at 34 °C and was held for 2 min. Then, it was heated at 50 °C/min to 300 °C. Mass spectrometry was operated with *m/z* ranging from 50 to 500. Species associated with each chromatographic peak were identified by comparing their observed mass spectrum with the NIST library. Results are normalised response to internal standard (IS). Change of analyte i was calculated according to:

$$\boldsymbol{Change}_i(\%) = 1 - \frac{(\boldsymbol{A}_i/\boldsymbol{A}_{IS})_{\boldsymbol{Final}}}{(\boldsymbol{A}_i/\boldsymbol{A}_{IS})_{\boldsymbol{Initial}}} * 100 \quad (3)$$

where A_i is the peak area of analyte i, and A_{IS} is the peak area of guaiacol added post-sampling. The absolute change in IS-normalised response is reported to capture effect size on the same measurement scale. For analyte i

$$\Delta\boldsymbol{Response}_i = (\boldsymbol{A}_i/\boldsymbol{A}_{IS})_{\boldsymbol{Final}} - (\boldsymbol{A}_i/\boldsymbol{A}_{IS})_{\boldsymbol{Initial}} \quad (4)$$

Negative values denote decreases; positive values denote increases. ΔResponse has the same (dimensionless) units as the table entries and complements 'Change (%)' by reflecting the magnitude of movement for abundant species.

The morphology of the electrodes and EDS (Energy-Dispersive X-Ray Spectroscopy) were acquired by TESCAN VEGA 3 Scanning Electron Microscope. Fourier transform infrared spectroscopy was carried out in a Shimadzu IRTracer-100 and scanned in transmittance mode. The scans were made 10 times from 500 to 4000 cm^{-1} with a resolution of 4 cm^{-1} with Happ-Genzel apodization. FTIR spectra were baseline-corrected and normalised.

For orientation, the electrical charge passed in a typical run was Q = 25.0 mA cm^{-2} * 4.0 cm^2 * 20 h = 2.00 Ah. Under PW_{NaCl}, using the tabled IS-normalised responses for phenol (Before = 0.049; After = 0.033), the conversion is X = 100*[1−(0.033/0.049)] = 32.7%. This corresponds to 32.7%/2.00 Ah = 16.3 Ah^{-1}. Whereas under PW_{TBAHFP}, responses were 0.0385 → 0.0205, i.e. X'=46.8% or 23.4% Ah^{-1}. This single worked example places the semi-quantitative metric on an electrochemical footing; because ionic strengths differ and iR was not measured.

3. Results

3.1. Electrochemical hydrogenation

Bio-oils are complex mixtures containing up to hundreds of compounds, therefore, only the largest peaks were identifiable and quantifiable via GC–MS. Tables 1 to 4 show the main peaks before and after the ECH of PW and WS with NaCl and TBAHFP, respectively, and will be referred to as PW_{NaCl}, PW_{TBAHFP}, WS_{NaCl} and WS_{TBAHFP}. The full composition tables can be found in the supplementary information (Tables S1–S4). Responses were normalised such that $A_{IS} = 1.00$. Due to the heterogeneous nature of the oil, the composition of each sample may vary in both concentration and compound distribution, which is reflected in the identifiable compounds in this study.

The IS-normalised response decreases reported here track substrate consumption rather than product formation. Most identifiable compounds showed decreases under the tested conditions, with phenolic species decreasing preferentially over ethers, ketones, and carboxylic acids, aligning with known reactivity trends in ECH [16,22,25]. This selectivity pattern, corroborated by independent FTIR evidence of reduced aromaticity and increased aliphatic character, is consistent with the ring hydrogenation pathway established for ECH of phenolics on Pt-group metals under mild conditions, and would be difficult to account for through physical losses such as evaporation or surface adsorption. Longer runs or parameter adjustments could increase the magnitude of the observed changes. The preferential decrease in phenolic responses over other oxygenated species has implications for bio-oil upgrading: increased saturation and deoxygenation correlate with higher heating value (HHV) and improved storage stability [26–29], both desirable outcomes from this process.

Hydrocarbons are mainly associated with the oily phase; in the aqueous phase they appeared at low levels [30]. For example, 2-methylnaphthalene and naphthalene were identified in PW_{NaCl}, while 3,7-dimethyl-decane was present in both WS_{NaCl} and WS_{TBAHFP}. The presence of these hydrocarbons highlights the chemical diversity of the oily phase and its potential as a precursor for the production of valuable chemicals.

Electrochemical hydrogenation of aromatic compounds proceeds via chemisorption of the π-system onto the metal surface in a near-planar geometry, followed by transfer of surface-adsorbed hydrogen (H*) to the ring [22,25,31,32]. Substituents adjacent to the reactive site sterically impede this flat-on adsorption, reducing the frequency and probability of surface contact. This effect is apparent when comparing structurally similar compounds, such as 2,5-dimethylphenol and 2,6-dimethylphenol (Fig. 2). Shifting a methyl group from the para to the ortho position reduced the response change from 46.03% to 36.59% (Table 1), consistent with increased steric obstruction of ring–surface interaction. A similar trend is seen in the ECH of PW_{TBAHFP} (Table 2),

Table 1
Semi quantitative composition of the main compounds in pinewood pyrolysis bio-oil oily phase with the addition of 1.5 g of NaCl before and after ECH. ΔResponse and Change (%) are calculated from IS-normalised responses (Ai/AIS). Values indicate the mean of triplicated experimental results. Values in brackets indicate the IS.

Compound	Before ECH (A_i/A_{IS})	After ECH (A_i/A_{IS})	ΔResponse	Change (%)
2,5-dimethyl-Phenol	0.063	0.034	0.029	46.03
Methyl propionate	0.05	0.028	0.022	43.64
2-methylnaphthalene	0.059	0.034	0.025	42.37
2,6-dimethyl-Phenol	0.123	0.078	0.045	36.59
p-Cresol	0.1	0.068	0.032	32.28
Phenol	0.049	0.033	0.016	31.53
Cyclopentanone	0.088	0.06	0.028	31.25
Naphthalene	0.099	0.072	0.027	27.27
Catechol	0.137	0.119	0.018	13.14
2-methoxy-Phenol	(1.000)	(1.000)	–	–

Table 2
Semi quantitative composition of the main compounds in pinewood pyrolysis bio-oil oily phase with the addition of 1.5 g of TBAHFP before and after ECH. ΔResponse and Change (%) are calculated from IS-normalised responses (Ai/AIS). Values indicate the mean of triplicated experimental results. Values in brackets indicate the IS.

Compound	Before ECH (A_i/A_{IS})	After ECH (A_i/A_{IS})	ΔResponse	Change (%)
Methanesulfonyl fluoride	0.0045	0.0013	0.0032	71.11
Phenol	0.0385	0.0205	0.018	46.75
p-Cresol	0.0766	0.0414	0.0352	45.95
2-methyl-Phenol	0.0475	0.0298	0.0177	37.26
2,4-dimethyl-Phenol	0.0424	0.0349	0.0075	17.69
Trimethyl phosphate	0.0263	0.091	−0.0647	−246.01
2-methoxy-Phenol	(1.000)	(1.000)	–	–

Table 3
Semi quantitative composition of the main compounds in wheat straw pyrolysis bio-oil oily phase with the addition of 1.5 g of NaCl before and after ECH. ΔResponse and Change (%) are calculated from IS-normalised responses (Ai/AIS). Values indicate the mean of triplicated experimental results. Values in brackets indicate the IS.

Compound	Before ECH (A_i/A_{IS})	After ECH (A_i/A_{IS})	ΔResponse	Change (%)
3,7-dimethyl-Decane	0.0431	0.033	0.0101	23.43
2-methyl-Phenol	0.2162	0.176	0.0402	18.59
2,6-dimethyl-Phenol	0.0453	0.038	0.0073	16.11
Phenol	0.3145	0.264	0.0505	16.06
Catechol	0.0979	0.085	0.0129	13.18
p-Cresol	0.3448	0.309	0.0358	10.38
2,3-dimethyl-Phenol	0.0362	0.034	0.0021	6.08
2-methoxy-Phenol	(1.000)	(1.000)	–	–

where phenol exhibited the highest percentage decrease (46.75%) compared to more branched phenolic compounds (Fig. 2), such as p-cresol (45.95%), 2-methylphenol (37.26%), and 2,4-dimethylphenol (17.69%). These results indicate that while methyl substitution does not completely prevent hydrogenation, increased steric hindrance can significantly reduce reactivity, consistent with previous observations [16].

The effect of molecular complexity is evident when comparing phenol and catechol in Table 1. Catechol, which has a second –OH group in the ortho position, showed a lower percentage decrease (13.14%) than phenol (31.53%), likely due to stronger intermolecular interactions and additional electronic effects that make hydrogenation more challenging. The same trend was observed for WS_{NaCl} (Table 3), where phenol showed a larger percentage decrease in IS-normalised response (16.06%) than catechol (13.18%). These results further suggests that the

Table 4
Semi quantitative composition of the main compounds in wheat straw pyrolysis bio-oil oily phase with the addition of 1.5 g of TBAHFP before and after ECH. ΔResponse and Change (%) are calculated from IS-normalised responses (Ai/AIS). Values indicate the mean of triplicated experimental results. Values in brackets indicate the IS.

Compound	Before ECH (A_i/A_{IS})	After ECH (A_i/A_{IS})	ΔResponse	Change (%)
2-ethyl-Phenol	0.01651	0	0.01651	100.00
3,7-dimethyl-Decane	0.06032	0.0378	0.02252	37.33
p-Cresol	0.39409	0.3385	0.05559	14.11
Phenol	0.31048	0.2947	0.01578	5.08
2-methyl-Phenol	0.19801	0.2115	−0.01349	−6.81
2-ethyl-4-methyl-Phenol	0.00002	0.0074	−0.00738	−100.00
Trimethyl phosphate	0.00007	0.5485	−0.54843	−100.00
2-methoxy-Phenol	(1.000)	(1.000)	–	–

number and position of functional groups influence the efficiency of ECH, with simpler phenolic structures undergoing hydrogenation more readily (See Fig. 2).

The observed changes (Table 1) in the response of methyl propionate (43.64%), 2-methylnaphthalene (42.37%), and cyclopentanone (31.25%) indicate the capability of the ECH process to upgrade not only phenolic compounds but also esters, hydrocarbons, and ketones. These results suggest that while phenolics are the most commonly reacted species under these conditions, other functional groups are also active, broadening the potential applications of ECH in bio-oil upgrading.

With TBAHFP, we observed fluorine- and phosphorus-containing species such as trimethyl phosphate (TMP) and methanesulfonyl fluoride. It is important to note that GC–MS analysis was not performed *in situ*; thus, interactions between the salt, electrolyte, and bio-oil components over time may have contributed to the formation of these new species. Additionally, the presence of these side products, relative to the main bio-oil components, may have caused peak overlap, reducing the number of identifiable compounds compared to PW_{NaCl}.

We treat TMP-mediated methylation as a working hypothesis rather than a confirmed mechanism, alongside alternatives such as methanolysis or transesterification. Within this context, increases in aliphatic C–H bands (≈2960/2850 cm^{-1}; Fig. 3) are consistent with alkylation of aromatic substrates, but ex-situ GC–MS and FTIR are not uniquely diagnostic [33].

From a processing standpoint, electrolyte-derived P-species represent secondary salt-solvent chemistry. Depending on the application, such species could add value or complicate purification; equally, their presence may contaminate product streams and necessitate additional separation or treatment. Here we treat these as system responses rather than desired products and discuss selectivity alongside electrolyte choice.

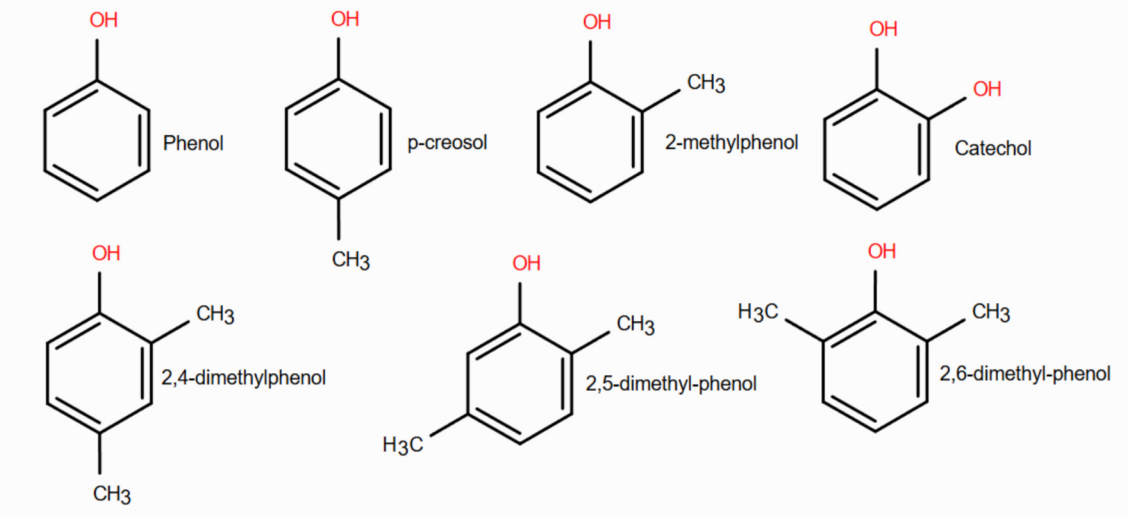

Fig. 2. Structures of some of the compounds present in pinewood and wheat straw bio-oils.

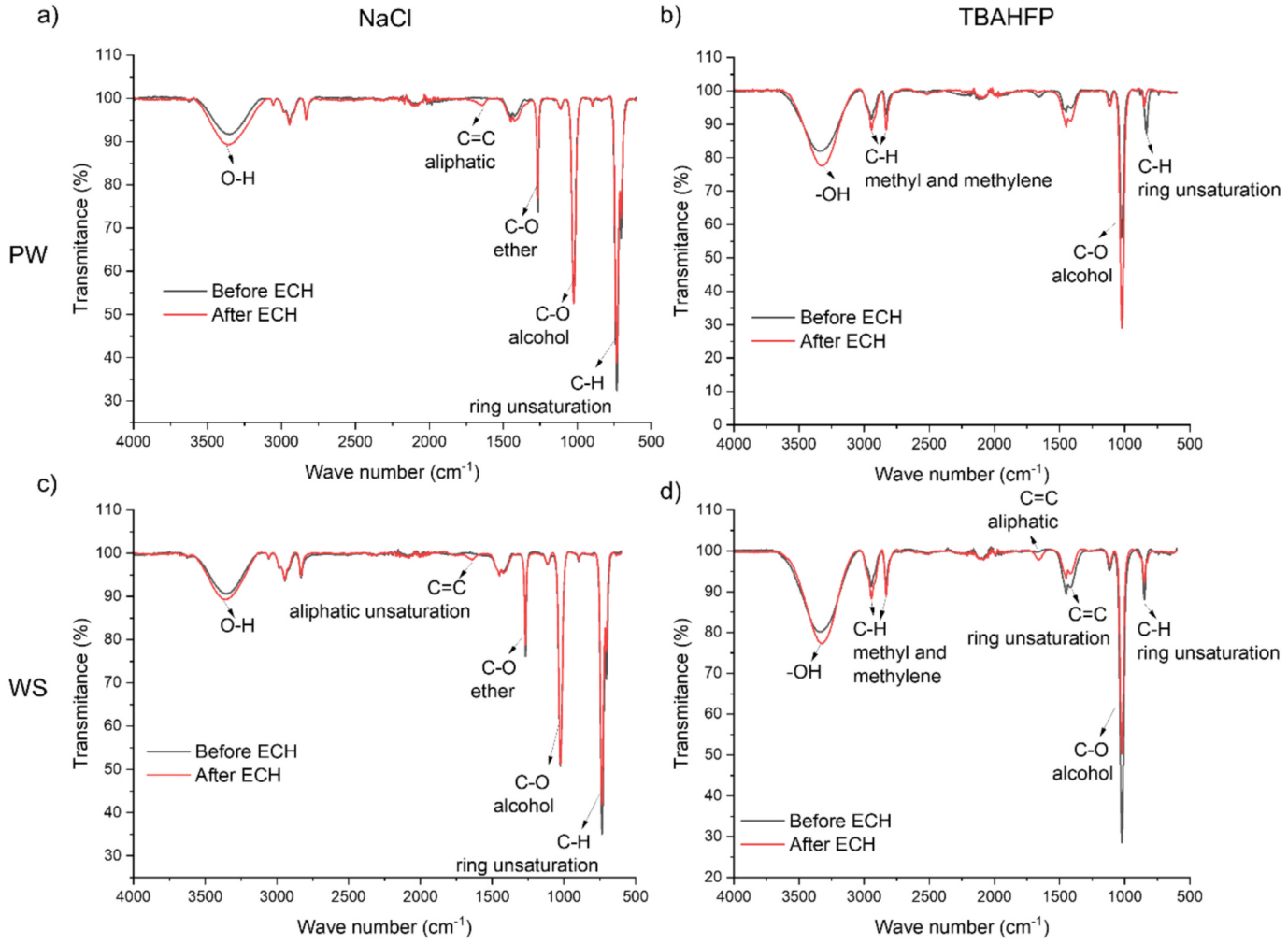

Fig. 3. FTIR spectra of (a) PW_{NaCl}, (b) PW_{TBAHFP}, (c) WS_{NaCl} and (d) WS_{TBAHFP} and the main identified organic functions, before (in black) and after (in red) the electrochemical process. (For interpretation of the references to colour in this figure legend, the reader is referred to the web version of this article.)

Consistent with the proposed methylation pathways, we observe formation of 2-ethyl-4-methylphenol and a 6.81% increase in the 2-methylphenol GC–MS response (Table 4; Fig. 4). Under TMP-promoted conditions, phenol and 2-ethylphenol undergo electrophilic aromatic substitution in which the phenolic –OH directs methylation to the ortho/para positions; methylation of phenol furnishes 2-methylphenol, while

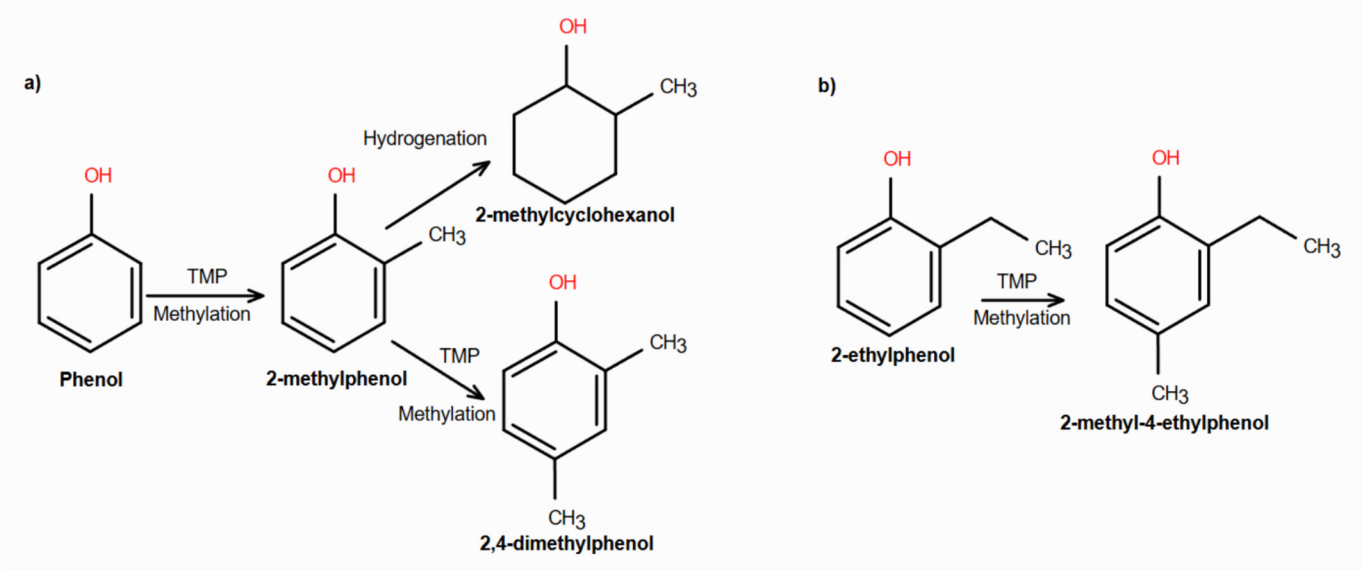

Fig. 4. Schematic representation of (a) the methylation of phenol and 2-methylphenol in the presence of TMP and the alternative hydrogenation path. (b) The methylation of 2-ethylphenol in the presence of TMP.

para-methylation of 2-ethylphenol yields 2-ethyl-4-methylphenol, as reported for lignin-derived phenolics. [33] In the same network, 2-methylphenol can act as both product and intermediate: a portion is diverted from hydrogenation to 2-methylcyclohexanol and instead undergoes further *para*-methylation to give 2,4-dimethylphenol (Fig. 4). The net effect is an apparent rise in the 2-methylphenol signal alongside accumulation of *para*-methylated products, consistent with TMP-driven methylation competing with aromatic ring hydrogenation.

3.2. FTIR analysis

FTIR spectroscopy was employed to characterise the chemical transformations occurring during the electrochemical hydrogenation of the oily phase. The spectra (Fig. 3) provided insights into functional group modifications, complementing the GC–MS findings and revealing trends in the broader chemical composition. Band assignments follow standard lignin/bio-oil literature (See Table 5); where bands overlap (e.g., 1657–1640 cm^{-}1), we report them as 'conjugated C=O/alkenic C=C' rather than assigning specific structures.

Reductions in the concentration of phenolics do not necessarily imply a decrease in total alcohol content, because mild ECH can hydrogenate the aromatic ring to cyclohexanols while conserving the hydroxyl group. In that case, the number of –OH groups (and thus the O–H FTIR envelope) may remain broadly unchanged. Where FTIR shows O–H growth, we ascribe it to concurrent pathways (e.g., methanolysis or formation of new alcohol environments) operating alongside ring hydrogenation.

The most prominent observation in Fig. 3 was the increase in the peak intensity within the 3200–3400 cm^{-1} region, which is indicative of O–H stretching vibrations in alcohols and phenols and was present in all four samples [34]. This is compatible with formation of additional O–H environments via hydrogenation of ketones, ethers, esters or carboxylic acids (Fig. 5) and/or alternative pathways such as methanolysis. The reduction of C-O alcohol groups was also observed in both mixtures with TBAHFP, where the peak at 1030 cm^{-1} decreased, likely due to dehydration reactions [34,35]. Both pyrolysis oil mixtures with NaCl presented a slight reduction in the peak related to C-O vibrations in ethers (1264 cm^{-1}) [34,36]. The hydrogenation of ethers could form –OH, contributing to the increase in alcohol content.

A further observation was the reduction of peaks corresponding to C–H vibrations in aromatic rings at 900 to 650 cm^{-1}.[37–39] The observed decrease is representative of reduced aromatic character and compatible with partial ring hydrogenation. These band changes are consistent with reduced aromaticity/increased aliphatic character, trends typically associated with higher energy density and stability [26–29].

Increases at 2960/2850 cm^{-1} are consistent with added aliphatic character and compatible with methylation, possibly promoted by TMP [34]. These are present in the mixtures with NaCl but only underwent a significant change with the addition of TBAHFP. A stronger peak near 1640 cm^{-1} appears post-ECH in PW_{NaCl}, WS_{NaCl} and WS_{TBAHFP}. This

Table 5
Assignment of FTIR bands.

Observed Peak (cm^{-1})	Band assignment	Specification	Ref.
625–900	C–H	Aromatic	37–39
1030	C-O	Primary alcohol	34–36
1264	C-O-C	Ether	34,36
1407	COO	Carboxylate	34
1508	C=C	Aromatic ring	35
1640	C=O/C=C	Unsaturated ketones, aldehydes, alkenic C=C	37,40
3000–2800	C–H	Methyl	34
3200	O–H	Alcohol (broad)	34

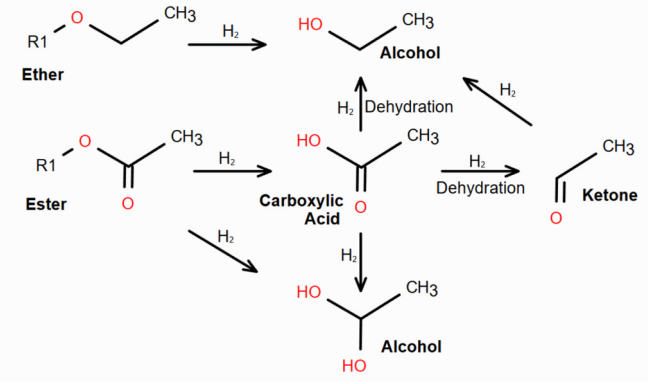

Fig. 5. Simplified schematic of the hydrogenation of several organic functional groups.

region can reflect alkenic C=C or conjugated C=O and is an indicator of changing unsaturation [37,40].

Table 6 shows all the observed changes in response for each functional group, assessed by either GC–MS or FTIR. Notably, the FTIR peak corresponding to the C-O bond in alcohols (1030 cm^{-1}) remained unchanged in mixtures containing NaCl. In contrast, it increased in WS_{TBAHFP} and decreased in PW_{TBAHFP}, underscoring the complexity of the electrochemical hydrogenation process.

Fig. 6 summarises the proposed reaction network, distinguishing pathways supported by compound-level GC–MS data from those inferred from FTIR functional-group trends.

4. Catalyst degradation

Scanning electron microscopy was utilised to understand the effect of both additives (NaCl and TBAHFP) on the corrosion of the catalytic cathode. Fig. 7 shows that, even in pristine conditions, that is, before any usage, the surface of the cathode already presented some black spots. Elemental mapping (by energy-dispersive X-ray spectroscopy) revealed that black spots correspond to sites where the coverage of deposited metals (platinum and ruthenium) was low, and the bare surface of the cathode (carbon) was visible. Our previous results [22] demonstrated that corrosion was not noticeable when the catholyte was sulfuric acid with model compounds, a more acidic media. Methanol is generally considered less aggressive than sulphuric acid and the observed degradation is consistent with salt effects under these conditions, though other contributions are possible.

After four ECH cycles (two with each oil) with NaCl as the additive, the catalyst surface exhibited signs of degradation. The SEM images (Fig. 8) revealed an increase in the blackened regions, and elemental mapping indicated a marked reduction in the platinum map intensity, accompanied by chlorine on the surface (in pink). Na is also visible; however, it was already present in the cathode before usage. In elemental mapping, the peaks for Cl and Ru are quite similar (at 2.622 keV and 2.559 keV, respectively) [41,42], suggesting that the high concentration of chlorine may have caused peak overlap with ruthenium; however, ruthenium remains present, as evidenced by its peak in the EDS spectrum (Fig. S1).

The co-occurrence of surface chlorine with reduced platinum signal is consistent with chloride-mediated degradation, but the present characterisation cannot distinguish between chemical attack and physical detachment of the catalyst layer with subsequent chloride adsorption on exposed carbon. The absence of comparable degradation in sulphuric acid under otherwise similar conditions [22] implicates the salt-methanol environment as a contributing factor. Such degradation could impair practical lifetimes, as it can compromise catalytic efficiency and raises concerns about the long-term economic viability of NaCl as an additive.

TBAHFP, often considered relatively benign toward noble metals in alcohol media, also caused surface damage after four cycles. Fig. 9 shows cracks and reduced platinum and ruthenium coverage, where only a few spots maintained PtRu deposition. It is worth noting that the cathode is built in layers, and SEM is representative of only the first layer. The cracks show that beneath the surface there is still metal coverage. However, the ECH process is a surface reaction dependent on direct contact of the metal with the unsaturated molecule, therefore this degradation would most likely result in the need for substitution of the material, however, long-term real-life studies would be necessary to confirm the extent of the damage.

The retained metal signal on the cathode surface was lower with TBAHFP than with NaCl. However, in PW_{TBAHFP}/WS_{TBAHFP} the FTIR data showed stronger O–H growth and reduced unsaturation, trends consistent with diminished aromaticity and increased aliphatic character. Literature links such shifts to higher HHV and improved storage stability across multiple upgrading routes [26–29]. Under these ionic strengths, supporting-electrolyte identity therefore sets a three-way trade-off among conversion, electrode stability, and product cleanliness (i.e., electrolyte-derived species).

These findings show that engaging the hydrophobic oily fraction by ECH is feasible under mild conditions, addressing a recognised gap in bio-oil upgrading. In practical terms, supporting-electrolyte choice becomes a process variable to be optimised: conductivity gains must be balanced against electrode durability and any effects on selectivity, framing the problem as multi-objective rather than single-metric.

Several of these findings are expected to generalise beyond the PtRu/ACC system. The finding that the oily fraction can be upgraded under mild conditions in methanol, the preferential reactivity of phenolics (consistent with their established adsorption thermodynamics on a range of transition metals), and the trade-off framework linking conversion, electrode stability, and product cleanliness provide transferable design principles for oily-phase ECH. Product selectivity and degradation kinetics, however, will be catalyst-dependent and should be mapped for alternative electrode materials in future work.

4.1. Comparison with the aqueous-phase system

A comparison with our previous aqueous-phase study [16] contextualises the present results and highlights the distinct challenges of oily-phase ECH. In the aqueous system (1 M H_2SO_4, 55 °C, 5 h), phenol decreased by 29.57%, p-cresol by 62.10%, and 2-methylphenol by 55.73%. In the oily phase under PW_{TBAHFP} (methanol, 55 °C, 20 h) the values were 46.75%, 45.95%, and 37.26% while under PW_{NaCl}, the corresponding decreases were 31.53%, p-creosol was not detected, and 36.59%. For most shared compounds, the aqueous phase achieved higher percentage decreases in a quarter of the run time, reflecting fundamental differences in the electrochemical environment.

Several factors contribute to this performance gap. First, the ionic conductivity of 1 M H_2SO_4 is substantially higher than that of NaCl or TBAHFP in methanol, where the low dielectric constant of the solvent limits ion mobility and dissociation [21]. Second, the local proton concentration at the cathode surface differs markedly between the two systems. In the aqueous system, the catholyte itself provides a high concentration of H^+ directly at the electrode surface; as protons are consumed by reduction to adsorbed hydrogen (H*), they are immediately replenished from the bulk acid. In the methanol system, the catholyte contains no acid, so protons must migrate through the membrane from the acidic anolyte. The local H^+ concentration at the cathode is therefore governed by the membrane transport rate, which may limit the rate of H* formation and, consequently, substrate hydrogenation. Third, the aqueous-phase study was conducted in strong acid, which did not cause noticeable corrosion of the PtRu/ACC cathode [22], whereas both NaCl and TBAHFP caused progressive surface damage in methanol,

Table 6
Every observed change in signal intensity/trend for organic functional groups (FTIR) and in IS-normalised responses (GC–MS). A "-" sign denotes 'not observed' in the respective bio-oil.

Content	WS_{NaCl}	PW_{NaCl}	WS_{TBAHFP}	PW_{TBAHFP}
Phenolic content	Decreased	Decreased	Decreased	Decreased
Ketones	–	Decreased	Decreased	–
Ethers	–	Decreased	Decreased	–
Esters	Decreased	Decreased	–	–
Carboxylic Acids	–	–	Increased	Increased
Aromatic C–H	Decreased	Decreased	Decreased	Decreased
C-O bands (alcohol ~ 1030 cm^{-1})	No change	No change	Decreased	Increased
C-O bands (ether ~ 1264 cm^{-1})	Decreased	Decreased	Decreased	Increased
Hydroxyls (–OH)	Increased	Increased	Increased	Increased
C=O/ alkenic C=C	Increased	Increased	Increased	Decreased
Hydrocarbons	–	Decreased	Decreased	–
Aliphatic C–H (2960/2850 cm^{-1})	No change	No change	Increased	Increased

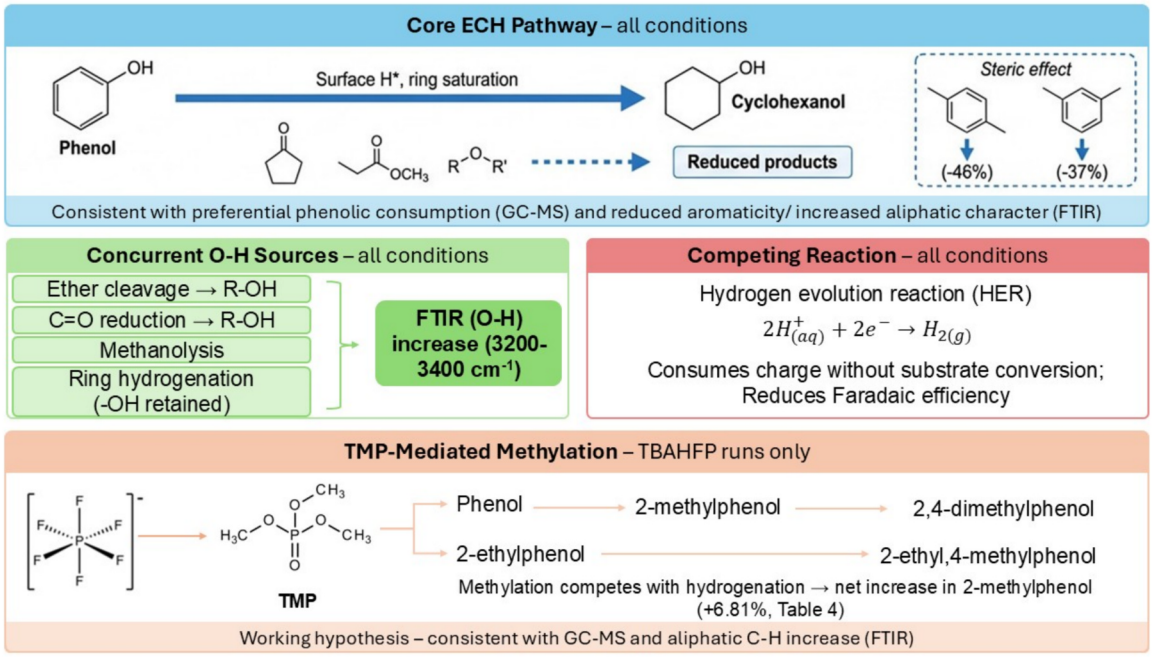

Fig. 6. Competing reactions scheme, where the hydrogenation pathway is highlighted in blue, the sources of O–H are in green, hydrogen evolution reaction is in red and the TPM-derived methylation is in orange. (For interpretation of the references to colour in this figure legend, the reader is referred to the web version of this article.)

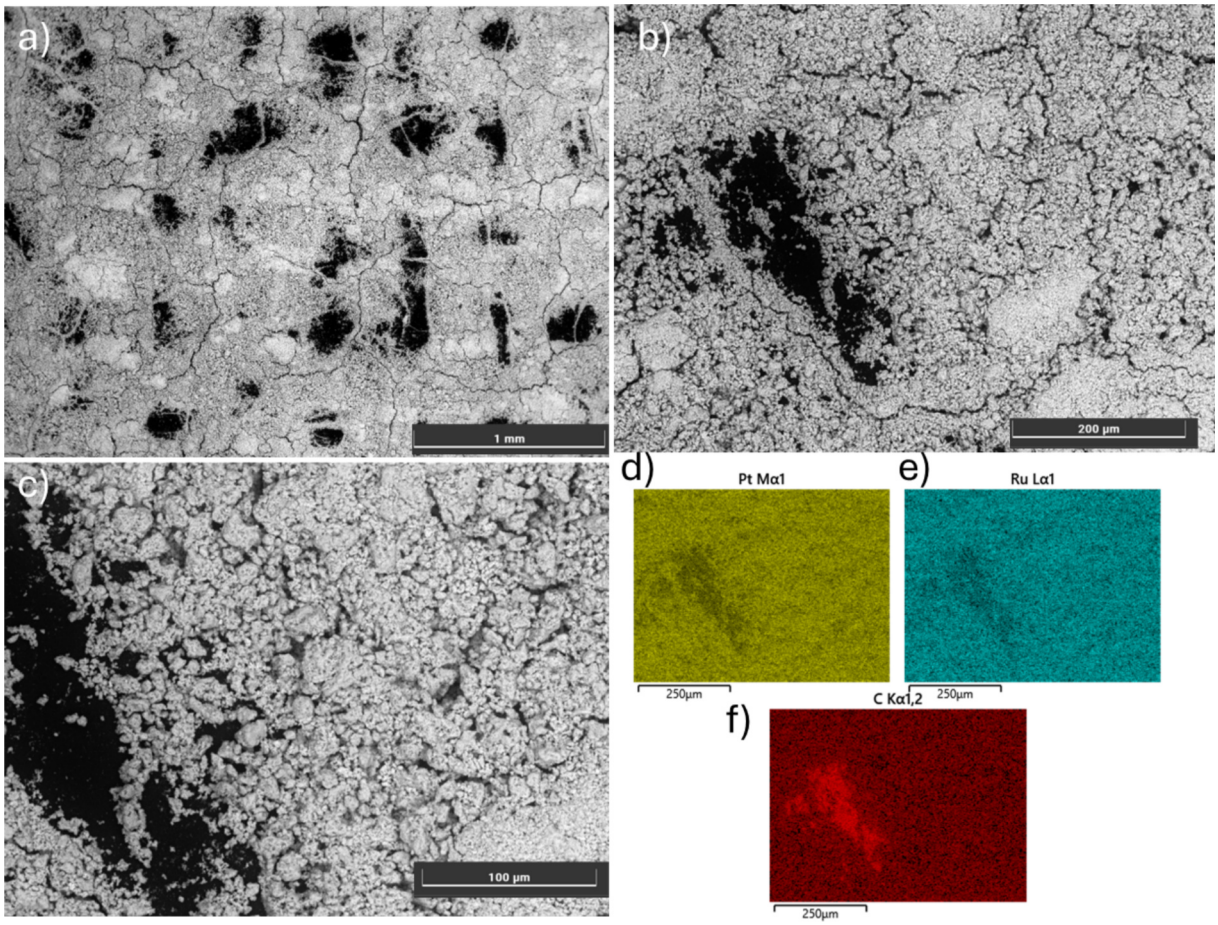

Fig. 7. Scanning Electron Microscopy of the cathode before the ECH process at three different magnifications (a-c) and elemental mapping of (d) platinum (in yellow), (e) ruthenium (in teal) and (f) carbon (in red). (For interpretation of the references to colour in this figure legend, the reader is referred to the web version of this article.)

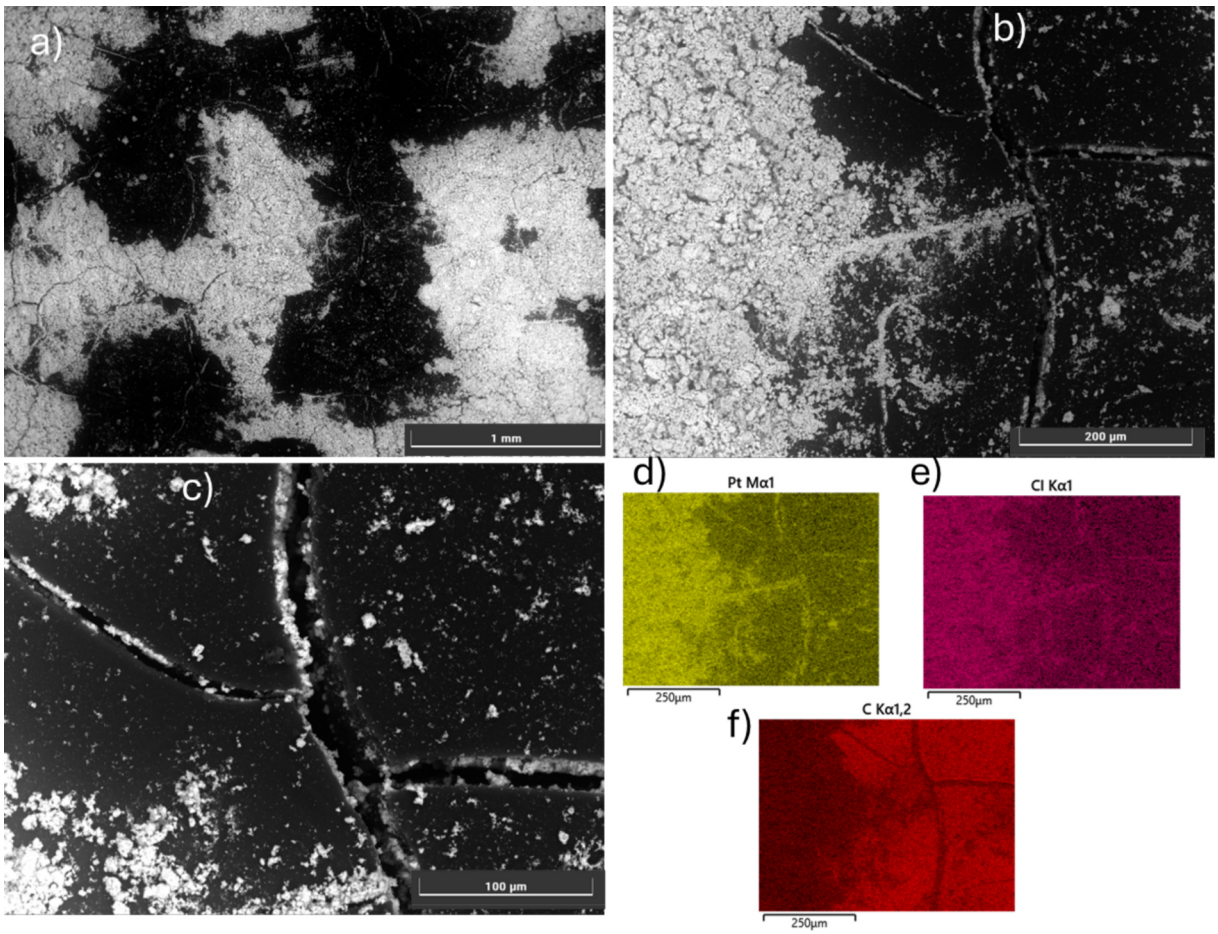

Fig. 8. Scanning Electron Microscopy of the cathode after four reruns (twice with PW_{NaCl} and twice with WS_{NaCl}) of the ECH process at three different magnifications (a-c) and elemental mapping of (d) platinum (in yellow), (e) chlorine (in pink) and (f) carbon (in red). (For interpretation of the references to colour in this figure legend, the reader is referred to the web version of this article.)

likely reducing catalytic activity over the course of each run.

Despite these kinetic disadvantages, the organic co-solvent approach achieves measurable and selective compositional changes in a fraction that is entirely inaccessible to purely aqueous ECH. The oily phase separates from aqueous electrolytes on contact and cannot be processed in conventional aqueous H-type cells. The only prior demonstration of oily-phase ECH [18] required elevated temperature and pressure to overcome this barrier. The present results show that a methanol-based catholyte can engage the oily fraction under mild conditions, at the cost of lower conversion rates and the need to manage additive-related degradation. While methanol was selected here for its electrochemical compatibility and miscibility with oily-phase constituents, other organic solvents or solvent–water mixtures could serve the same function and may offer improved conductivity or proton availability. A methanol–-water co-solvent system could potentially enable simultaneous processing of both bio-oil fractions in a single cell, an approach worth investigating in future work. Additive selection and electrode durability remain the key variables to optimise for practical implementation.

5. Conclusion

This study explored the electrochemical hydrogenation of the oily phase of wheat straw and pinewood pyrolysis bio-oils using a PtRu/ACC catalyst and methanol-based catholytes with NaCl and TBAHFP as conductive additives. The findings provide insights into optimising ECH processes to address the solubility and conductivity challenges associated with bio-oil upgrading.

The results demonstrated that phenolic compounds, which dominate the composition of the oily phase, are preferentially consumed during ECH, with GC–MS and FTIR trends consistent with ring saturation, changes typically associated with higher energy density and stability [26–29]. Methanol served as an effective catholyte for dissolving the hydrophobic oily phase, enabling the direct electrochemical conversion of its compounds. However, its low conductivity required the addition of conductive salts, highlighting a fundamental trade-off between enhanced conductivity and electrode stability. NaCl at ~ 0.29 M raises ionic strength but introduces chloride-linked degradation. TBAHFP at ~ 0.04 M avoids chloride yet can promote side reactions (e.g., P-containing species) and still led to notable surface damage. Accordingly, additive choice should be tailored to the desired balance between conversion, stability and product cleanliness.

From a broader perspective, the insights gained in this study inform the feasibility of ECH as a green and scalable approach for bio-oil upgrading. By operating under mild conditions, this process operates under conditions compatible with the principles of green chemistry, offering a sustainable alternative to high-pressure catalytic hydrogenation methods. However, the observed trade-offs between efficiency and material stability emphasise the importance of developing novel additives and electrode materials tailored for the specific demands of bio-oil conversion.

Future research should focus on designing conductive additives that minimise degradation while maintaining reaction efficiency, screening alternative electrode materials for improved durability, and investigating solvent–water co-solvent systems that could enable simultaneous processing of both bio-oil fractions. By addressing these challenges, ECH has the potential to contribute to renewable fuel production from

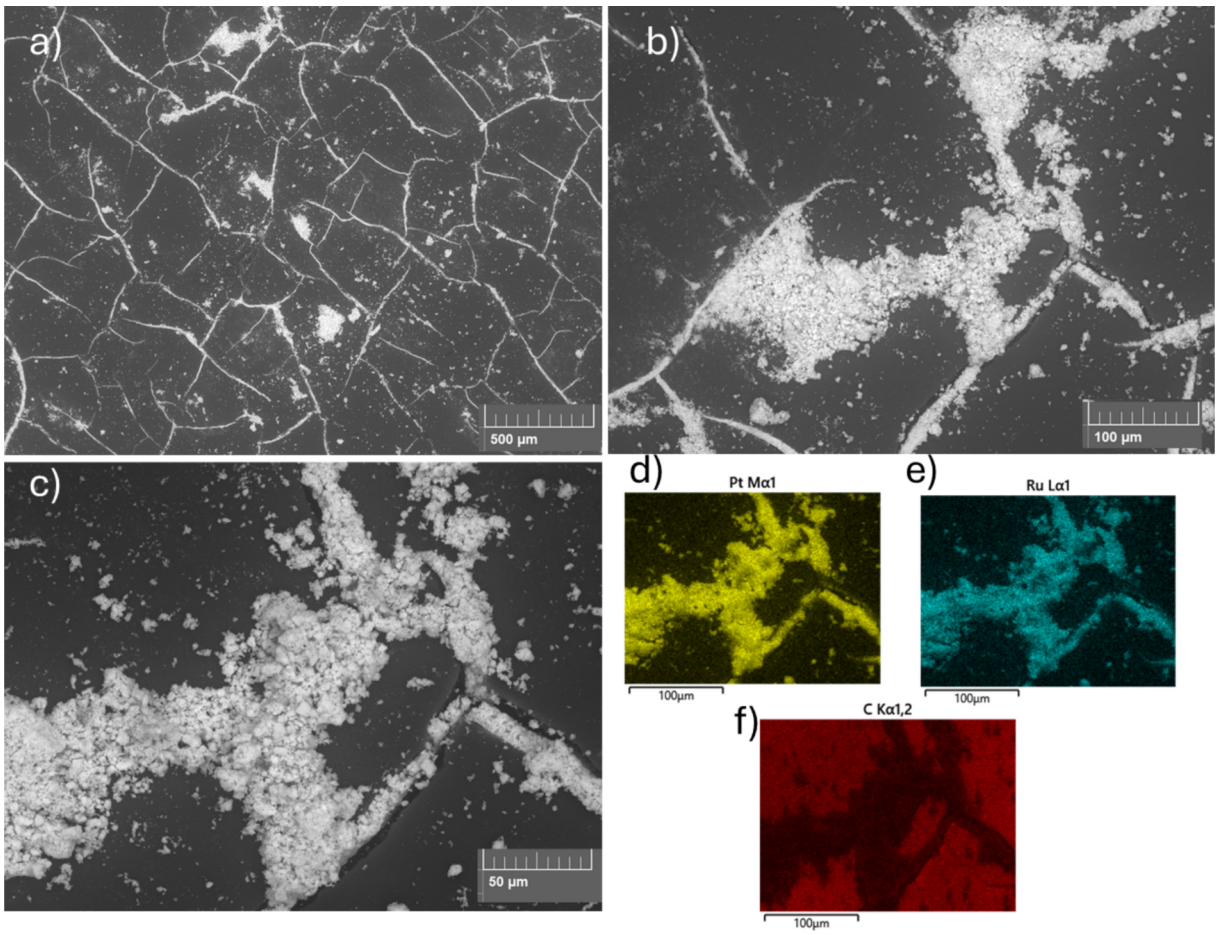

Fig. 9. Scanning Electron Microscopy of the cathode after four reruns (twice with PW_{TBAHFP} and twice with WS_{TBAHFP}) of the ECH process at three different magnifications (a-c) and elemental mapping of (d) platinum (in yellow), (e) ruthenium (in teal) and (f) carbon (in red). (For interpretation of the references to colour in this figure legend, the reader is referred to the web version of this article.)

biomass.

Author contribution

C. Catizane conducted the experimental work and analysis/imaging and was the primary author of the paper. J. Sumner and Y. Jiang supervised the research, revised the manuscript and contributed to the technical content of the paper. S. Banks and S. Mori revised the manuscript and contributed to the technical content of the paper.

CRediT authorship contribution statement

Cesar Catizane: Writing – review & editing, Writing – original draft, Visualization, Validation, Project administration, Methodology, Investigation, Formal analysis, Data curation, Conceptualization. **Ying Jiang:** Writing – review & editing, Supervision, Project administration, Funding acquisition, Conceptualization. **Scott Banks:** Writing – review & editing, Resources, Funding acquisition. **Joy Sumner:** Writing – review & editing, Supervision, Project administration, Funding acquisition, Conceptualization. **Stefano Mori:** Writing – review & editing, Supervision, Funding acquisition.

Declaration of competing interest

The authors declare that they have no known competing financial interests or personal relationships that could have appeared to influence the work reported in this paper.

Acknowledgements

The authors are grateful for the pyrolysis liquid supplied for this research from the Biochar CleanTech Accelerator project. Innovate UK Project No: 10055261. The authors wish to thank UK EPSRC (EP/T518104/1) for supporting the work published in the paper through an EPSRC Doctoral Training Partnership Funding.

Appendix A. Supplementary data

Supplementary data to this article can be found online at https://doi.org/10.1016/j.fuel.2026.140168.

Data availability

I have shared the link to my data in the document.

The source data supporting this study's findings are available from the Figshare repository (10.6084/m9.figshare.30520913).

References

[1] Chang, S. H. Plastic waste as pyrolysis feedstock for plastic oil production: A review. https://doi.org/10.1016/j.scitotenv.2023.162719 (2023) doi:10.1016/j.scitotenv.2023.162719.

[2] Hansen S, Mirkouei A, Diaz LA. A comprehensive state-of-technology review for upgrading bio-oil to renewable or blended hydrocarbon fuels. Renew Sustain Energy Rev 2020;118:109548.

[3] Wang K, et al. Electroreductive upgradation of biomass into high-value chemicals and energy-intensive biofuels. Green Chem 2024;26:2454–75.

[4] Kumar R, Strezov V. Thermochemical production of bio-oil: a review of downstream processing technologies for bio-oil upgrading, production of hydrogen and high value-added products. Renew Sustain Energy Rev 2021;135:110152.

[5] Graca, I., Lopes, J. M., Cerqueira, H. S. & Ribeiro, M. F. Bio-oils Upgrading for Second Generation Biofuels. *Ind. Eng. Chem. Res.* **52**, 275–287 (2012).

[6] Adjaye JD, Bakhshi NN. Catalytic conversion of a biomass-derived oil to fuels and chemicals I: model compound studies and reaction pathways. Biomass Bioenergy 1995;8:131–49.

[7] Mortensen PM, Grunwaldt JD, Jensen PA, Knudsen KG, Jensen AD. A review of catalytic upgrading of bio-oil to engine fuels. Appl Catal A 2011;407:1–19.

[8] Chen G, et al. Upgrading of bio-oil model compounds and bio-crude into biofuel by electrocatalysis: a review. ChemSusChem 2021;14:1037–52.

[9] Page JR, Manfredi Z, Bliznakov S, Valla JA. recent progress in electrochemical upgrading of bio-oil model compounds and bio-oils to renewable fuels and platform chemicals. Materials 2023;16:394.

[10] Garedew M, Young-Farhat D, Jackson JE, Saffron CM. Electrocatalytic upgrading of phenolic compounds observed after lignin pyrolysis. ACS Sustain Chem Eng 2019;7:8375–86.

[11] Zhou Y, et al. Electrocatalytic upgrading of lignin-derived bio-oil based on surface-engineered PtNiB nanostructure. Adv Funct Mater 2019;29:1807651.

[12] Lam, C. H. *et al.* Electrocatalytic upgrading of model lignin monomers with earth abundant metal electrodes. **17**, 601 (2015).

[13] Roessler A, Dossenbach O, Rys P. Electrocatalytic Hydrogenation of Indigo. J Electrochem Soc 2003;150:D1.

[14] Du Y, Chen X, Liang C. Selective electrocatalytic hydrogenation of phenols over ternary Pt3RuSn alloy. Mol Catal 2023;535.

[15] Li Z, et al. A mild approach for bio-oil stabilization and upgrading: electrocatalytic hydrogenation using ruthenium supported on activated carbon cloth. Green Chem 2014;16:844–52.

[16] Catizane, C., Jiang, Y., Banks, S. & Sumner, J. Pinewood and wheat straw bio-oil aqueous phase electrochemical hydrogenation utilising a PtRu/ACC catalyst. *Sustain. Energy Fuels* https://doi.org/10.1039/D5SE00965K (2025) doi:10.1039/D5SE00965K.

[17] Zhang B, Zhang J, Zhong Z. Low-energy mild electrocatalytic hydrogenation of bio-oil using ruthenium anchored in ordered mesoporous carbon. ACS Appl Energy Mater 2018;1:6758–63.

[18] Pelosin P, et al. High-temperature high-pressure electrochemical hydrogenation of biocrude oil. Renew Energy 2024;222:119899.

[19] Alsalem MM, Camilla S, Ryan MP, Sedransk Campbell K. Understanding the role of NaCl concentration on the corrosion of carbon steel and $FeCO_3$ formation in CO_2 -containing electrolytes. Ind Eng Chem Res 2021;60:12032–48.

[20] Peng J, et al. Effect of boiling pretreatment on physicochemical and transport properties of perfluorosulfonic acid membrane. ACS Appl Polym Mater 2023;5:9940–51.

[21] Dorn M, Kareth S, Weidner E, Petermann M. Electrical conductivity of lithium, sodium, potassium, and quaternary ammonium salts in water, acetonitrile, methanol, and ethanol over a wide concentration range. J Chem Eng Data 2024;69:1493–502.

[22] Catizane C, Jiang Y, Sumner J. Mechanisms of electrochemical hydrogenation of aromatic compound mixtures over a bimetallic PtRu catalyst. Commun Chem 2025;8:56.

[23] Long Y, et al. Corrosion behaviour of T92 steel in NaCl solution. Int J Electrochem Sci 2017;12:5104–20.

[24] Creager, S. Solvents and Supporting Electrolytes. in *Handbook of Electrochemistry* 57–72 (Elsevier, 2007). doi:10.1016/B978-044451958-0.50004-5.

[25] Catizane C, Jiang Y, Sumner J. Hydrogen bond enhanced electrochemical hydrogenation of benzoic acid over a bimetallic catalyst. Sustain Energy Fuels 2025;9:3014–22.

[26] Wang H, Male J, Wang Y. Recent advances in hydrotreating of pyrolysis bio-oil and its oxygen-containing model compounds. ACS Catal 2013;3:1047–70.

[27] Han Y, et al. Hydrotreatment of pyrolysis bio-oil: a review. Fuel Process Technol 2019;195:106140.

[28] Channiwala SA, Parikh PP. A unified correlation for estimating HHV of solid, liquid and gaseous fuels. Fuel 2002;81:1051–63.

[29] Oh S, Lee JH, Choi JW. Hydrodeoxygenation of crude bio-oil with various metal catalysts in a continuous-flow reactor and evaluation of emulsion properties of upgraded bio-oil with petroleum fuel. Renew Energy 2020;160:1160–7.

[30] Catizane C, Jiang Y, Sumner J. Improving plastic pyrolysis oil quality *via* an electrochemical process for polymer recycling: a review. Energy Adv 2024;3:366–88.

[31] Li G, Han J, Wang H, Zhu X, Ge Q. Role of dissociation of phenol in its selective hydrogenation on Pt(111) and Pd(111). ACS Catal 2015;5:2009–16.

[32] Honkela ML, Björk J, Persson M. Computational study of the adsorption and dissociation of phenol on Pt and Rh surfaces. PCCP 2012;14:5849.

[33] Duval A, Avérous L. Mild and controlled lignin methylation with trimethyl phosphate: towards a precise control of lignin functionality. Green Chem 2020;22:1671–80.

[34] Lv P, Almeida G, Perré P. TGA-FTIR analysis of torrefaction of lignocellulosic components (cellulose, xylan, lignin) in isothermal conditions over a wide range of time durations. BioResources 2015;10.

[35] Gallio E, et al. Fourier transform infrared spectroscopy in treated woods deteriorated by a white rot fungus. Maderas Ciencia y tecnología 2018;0–0. https://doi.org/10.4067/S0718-221X2018005031701.

[36] Sammons RJ, et al. Characterization of Organosolv Lignins using thermal and FT-IR Spectroscopic Analysis. BioResources 2013;8.

[37] Sun R, Tomkinson J. Comparative study of lignins isolated by alkali and ultrasound-assisted alkali extractions from wheat straw. Ultrason Sonochem 2002;9:85–93.

[38] Rao CNR, Venkataraghavan R. Contribution to the infrared spectra of five-membered n- and n s-heterocyclic compounds. Can J Chem 1964;42:43–9.

[39] Margoshes M, Fassel VA. The infrared spectra of aromatic compounds. Spectrochim Acta 1955;7:14–24.

[40] Stankovikj F, McDonald AG, Helms GL, Garcia-Perez M. Quantification of bio-oil functional groups and evidences of the presence of pyrolytic humins. Energy Fuel 2016;30:6505–24.

[41] X-ray Transition Energies Search Form. https://physics.nist.gov/PhysRefData/XrayTrans/Html/search.html.

[42] Bearden JA. X-ray wavelengths. Rev Mod Phys 1967;39:78–124.

https://dspace.org/

Electrochemical hydrogenation of the hydrophobic oily phase of pinewood and wheat-straw pyrolysis oils in methanol

Catizane, Cesar; Jiang, Ying; Banks, Scott; Sumner, Joy; Mori, Stefano

2027-01-15
Elsevier
https://doi.org/10.1016/j.fuel.2026.140168
Catizane C, Jiang Y, Banks S, et al., (2027) Electrochemical hydrogenation of the hydrophobic oily phase of pinewood and wheat-straw pyrolysis oils in methanol. Fuel, Volume 428, Part B, January 2027, Article number 140168

Downloaded from a DSpace repository. https://dspace.org/